Mach-Zehnder Interferometer progress report

David Paredes Barato[1,*]

[1]*Department of Physics, Durham University, Rochester Building, South Road, Durham DH1 3LE, United Kingdom*

(Dated: February 1, 2011)

In this report we will review the work that has been carried out in this first term related to the project "Single photon interactions with a superatom". Furthermore, the construction of a Mach-Zehnder interferometer that will eventually be used in the main Rydberg experiment is documented.

Keywords: Mach-Zehnder Interferometer, homodyne detection, single photon detection

I. INTRODUCTION

The objective of the piece of equipment that I'm developing is to be able to discern the signal of a single photon in our experiment, where we use a coherent beam to excite a cloud of atoms to the Rydberg Blockade regime. This should be, in principle, achievable using a Mach-Zehnder Interferometer (MZI) as the basis of homodyne detection.

A normal MZI splits an input beam into two paths using a 50:50 beam splitter (BS), one of which will propagate freely and the other will undergo a phase shift produced by the physical effect of interest. Then, these two beams combine in another BS giving rise to interference between the two beams. The differential signal of the two beams thus produced is proportional to the phase difference between the two arms of the interferometer (see Figure 4)

We can *scan* the phase difference between the two paths by changing slightly and in a controlled manner the optical path length of one of the arms, introducing –for example– a thick glass plate and rotating it, or using a piezoelectric transducer (PZT) mounted on one of the mirrors to alter the path length of propagation of one of the beams.

There is, however, a problem related to these kind of interferometers: as these are sensitive to small changes in optical path (of the order of the wavelength), there are many sources of noise, such as changes in density of the surrounding air, small mechanical vibrations, temperature expansion of the parts, etc. Therefore, stabilization of the interferometer is of the utmost importance.

In this report I will review some of the theory behind homodyne detection and the experimental device divided in the detector, source and main interferometer stages.

A. Theory of Homodyne detection

An interferometer is a device which can obtain information from waves obeying the superposition principle. If we apply this to EM waves, we will obtain changes in intensity based on the superposition of the electric field. Generally speaking, the information we are interested in is encoded in the interference pattern formed when two or more electromagnetic fields occupy the same volume in spacetime.

In our case, our Mach-Zehnder interferometer will be used to get information about the phase change undergone by the light passing through one of its arms by means of homodyne detection; i.e., we will compare the outputs of the last BS to get information about the quadratures of the field of interest. To be in the so-called strong local oscillator (LO) regime, we will split the input beam in such a way that the light passing through the probe arm is much weaker than in the other.

In a two-port homodyne detection scheme (with a lossless 50-50 BS, as shown in Figure 1) we get rid of the non-interacting terms by substracting the signal at both outputs and retain the interference terms [1–4].

Following the arguments of [1] we can represent a single-mode electric field as

$$E(r,t) = \frac{\mathrm{i}}{\sqrt{2}}\left(a e^{-\mathrm{i}(k\cdot r-\omega t)} + h.c\right) \quad (1)$$

$$= a_1 \cos(k\cdot r-\omega t) + a_2 \sin(k\cdot r-\omega t) \quad (2)$$

where $a = a_1 + \mathrm{i}a_2$ is the anihilation operator of the field mode, and its real and imaginary parts are the quadrature-phase operators.

If we denote by a and b anihilation operators for the input ports 1 and 2, and c and d for the output ports 3 and 4 of the BS (see Figure 1), we can express the evolution of these operators via the evolution operator U

$$\begin{pmatrix} c \\ d \end{pmatrix} = U \begin{pmatrix} a \\ b \end{pmatrix} \quad (3)$$

where the coefficients of U,

$$U = \begin{pmatrix} \mathcal{R} & \mathcal{T} \\ \mathcal{T} & -\mathcal{R}^* \end{pmatrix}, \quad (4)$$

are complex numbers that satisfy $|\mathcal{R}|^2 + |\mathcal{T}|^2 = 1$.

We can describe the anihilation operator a as the sum of its mean field $A = \langle a \rangle$ and the noise carrying part, $a - \langle a \rangle \equiv$

*david.paredes@durham.ac.uk

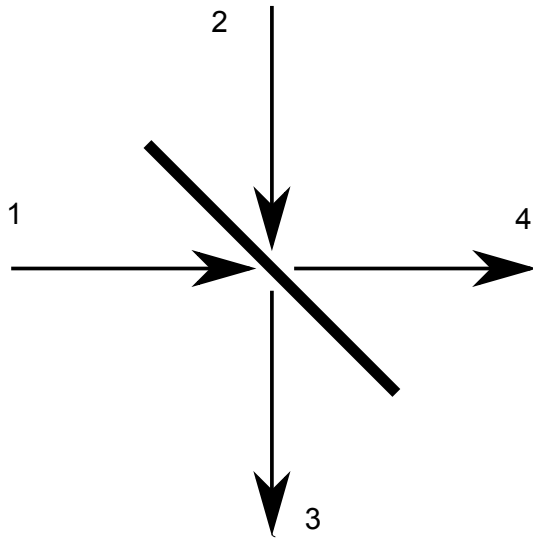

FIG. 1: Beamsplitter scheme: input channels are 1 and 2, whereas output channels are 3 and 4.

Δa. Shifting the phase of the reflection coefficients such that the mean value of the anihilator operator for the LO, b, multiplied by this phase is a real number, we can see that

$$a = A + \Delta a = A_1 + iA_2 + \Delta a_1 + i\Delta a_2 \quad (5)$$
$$b = B + \Delta b = B + \Delta b_1 + i\Delta b_2. \quad (6)$$

There are some operators that are of interest for the analysis of the output of the BS:

- Number operator, proportional to the intensity: $\langle N_a \rangle = \langle a^\dagger a \rangle$
- Noise number operator, proportional to the noise intensity: $\langle N_{\bar{a}} \rangle = \langle \Delta a^\dagger \Delta a \rangle$
- Intensity fluctuations: $\langle \Delta N_a^2 \rangle = \langle N_a^2 \rangle - \langle N_a \rangle^2$

An account of these expressions for the quantities associated to different inputs (Fock state, coherent state,...) can be obtained in [1]. The outputs obtained from channels 3 and 4 are proportional to $N_c = c^\dagger c$ and $N_d = d^\dagger d$, the homodyne photocurrent for a 50-50 BS is

$$\langle P \rangle = \langle a^\dagger b + b^\dagger a \rangle = 2BA_1 \quad (7)$$

and the noise is, in the strong LO limit

$$\langle \Delta P^2 \rangle \approx 4B^2 \Delta a_1^2 \quad (8)$$

If we adjust the phase in the combination $P(\theta) = N_c \cos\theta + N_d \sin\theta$ of the two photodetectors we can observe Δa_1^2, Δa_2^2 or any combination of the two.

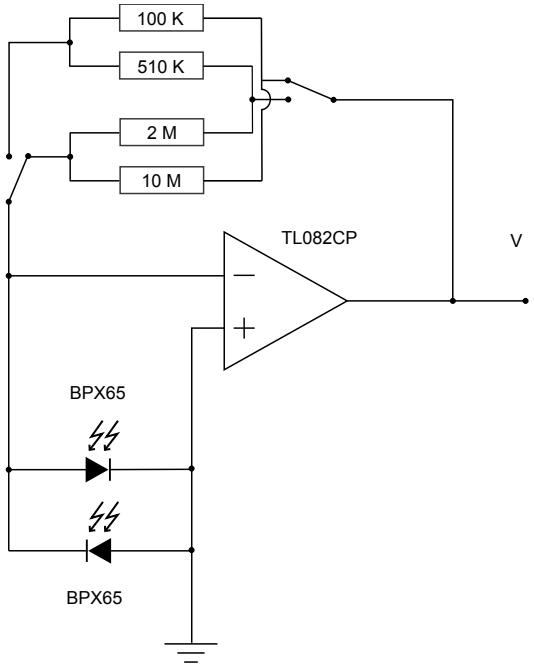

FIG. 2: Differential balanced photodetector layout

II. EXPERIMENTAL DEVICE

The experiment, which is being carried out in the laboratory 54, will be taken to laboratory 56 at some point. Until that moment, the laser source I am using will be different from the one used in the main experiment, as well as the definitive dimensions of the interferometer and final layout. Therefore, I've tried to maintain modularity in the experiment, so that one can work on each of the parts of the experiment separately without greatly disturbing the rest.

A. Detection stage

The main detector is a custom built differential balanced photodetector (DPD) based on the operational amplifier TL082CP and two back-to-back BPX65 photodiodes (PD), whose amplification is varied by switching between resistors of different values. The layout for the connections of the DPD can be seen in Figure 2.

The operational amplifier was selected among other options because of its faster slew rate (and thus greater bandwidth) and is fed using two 9V batteries. The components are connected in a board and encased in a metallic case. The case has holes for the PD as well as the BNC which interfaces the DPD with the outside. The case is fixed on a standard optical mount pole.

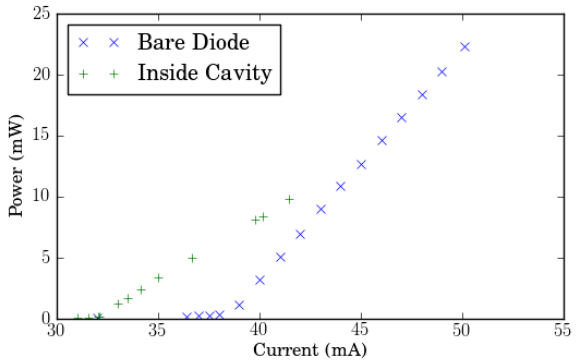

FIG. 3: Power profile as a function of current for the cases of the bare laser and the laser inside the external cavity.

B. Source stage

We are using a SHARP laser diode model GH0780MA2C with a wavelength of 784 nm for our coherent light source. It is mounted on a collimation tube and a holder with an external cavity formed by a diffraction grating connected to a PZT to allow wavelength tunability near the D2 line of ^{87}Rb.

Using the collimation tube we obtained a collimated beam with a waist of approximately 0.61 mm and a polarization parallel to the optical bench plane.

A Power vs. Current profile was obtained (see Figure 3) with and without the external cavity to ascertain that the lasing threshold is lowered by the introduction of the cavity because of the feedback from the grating.

For our laser diode, the working parameters under which the lasing happens at the D2 line are a current of $I = 43.83$mA and a temperature of $T = 19.52°$C.

Source stage and interferometer are connected using a fiber, as it allows more modularity in the design. Therefore, a $\lambda/2$ waveplate and an optical isolator are placed between the source and the fiber to minimize the amount of light reflected back to the laser once it is appropriately fiber coupled. The fiber is an OZ optics LPC-02-780-5/125-p-1.3-6.2AS-40-X-3-2.

III. INTERFEROMETER

An interferometer is a device that relies on the principle of superposition to analyze the waves that pass through it. The interference will appear at a certain point when two monochromatic waves with a certain phase coherence between them arrive at that point at the same time.

In our case we shall use an MZI in which a collimated beam is split in a BS into two beams of the same power. Then, two mirrors will direct the beam to another BS after which the beams will be collected by the DPD. Phase tunability will be obtained with a PZT attached to one of the mirrors and connected to an independent voltage source (see Figure 4).

As the power leaving the fiber is too high for the detector, we used a neutral density filter to attenuate the input of the MZI instead of the output. This has the advantage that we only have to attenuate one beam, but has the disadvantage that, in order to obtain a power which optimizes the detector's output, the beam is too weak to be seen even with the IR card. Therefore, we will align the MZI without the neutral density filter, and it will be introduced afterwards.

A. Alignment

Careful alignment should be performed on each section of the device.

The beam paths must always be parallel to the table and optical elements such as waveplates must be perpendicular to the beam to avoid translating it: in this way we will reduce the effort required to introduce a new optical element in the paths followed by the light.

On each BS we will make sure that the perpendicular reflections come out of this element parallel to the table. The mirrors will then direct the light towards the poing

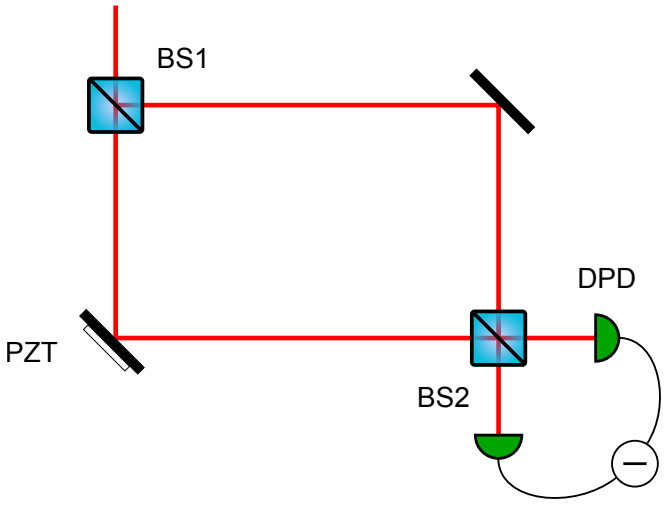

FIG. 4: Standard Mach-Zehnder interferometer layout. The piezoelectric transducer (PZT) allows phase tunability

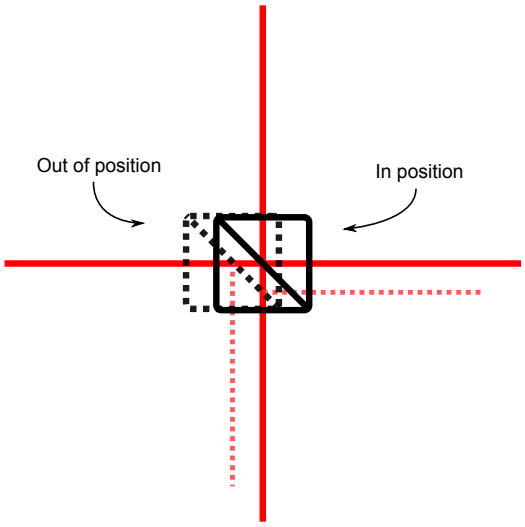

FIG. 5: Beamsplitter alignment. Once the movement is restricted to 1D, make sure that the output beams are parallel.

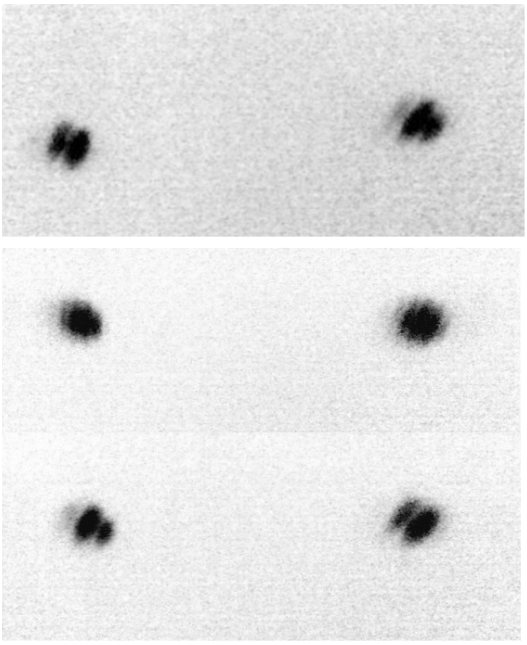

FIG. 6: Interferences appearing in both spots after the MZI. There are differences in the interference spacing as well as the orientation and visibility for different orientations of the BS.

where the second BS should be placed. The introduction of the second BS can be performed in the surroundings of that point, bearing in mind that the paths of the light coming out of it shall be parallel. If we restrict the movement of this BS to one dimension parallel to one of the paths, it is possible to obtain a careful alignment of the BS cube by comparing the close- and far-field position of the spots in both output channels, making sure they are leveled and parallel at all times(see Figure 5.

Once the orientation of the BS is adequate, we can displace the BS in the free dimension to bring the output spots together. When they are very close together, one of two things can happen:

- Fringes can appear within the illuminated area at the output ports.
- No fringes appearing, in which case we can block one of the paths to localize (if possible) a probable difference in illumination due to a small difference in positions. When blocking one of the input paths the illumination should decay uniformly within the spot. If there is an non-uniform, apreciable change in the spatial distribution of light within the spot, realignment is required.

When the fringes appear, they would have a definite orientation. We can imagine we are looking at a small part of a big interference pattern, so the fringes are narrower the further we are from the center and their orientation will tell us about the position of the "center", thus changing the orientation of the BS will allow us to reach the center of the interference pattern and therefore optimize the visibility.
There's a wealth of information about Mach-Zehnder interference phenomena using various sources and analyzing different applications in [5].

B. PZT

As we have pointed out, it is possible to tune the phase shift between the arms of the interferometer by using a PZT driving a mirror.
We drive the Thorlabs AE0203D04 PZT using a triangular wave from a 150V source with a monitor output at a frequency less than 100 Hz. In Figure 7 we can see that the correspondence between the monitor voltage and the output voltage is a straight line with slope $V_{out} \approx 9.7 V_{mon}$.

The small movements (on the order of the wavelength) let us scan the phase shift, thus showing a sinusoidal signal if we connect the output of the DPD to a osciloscope and trigger it with the signal driving the PZT.

C. All-air MZI

The layout of the all-air MZI is depicted in Figure 4. The light entering the interferometer is the output of the

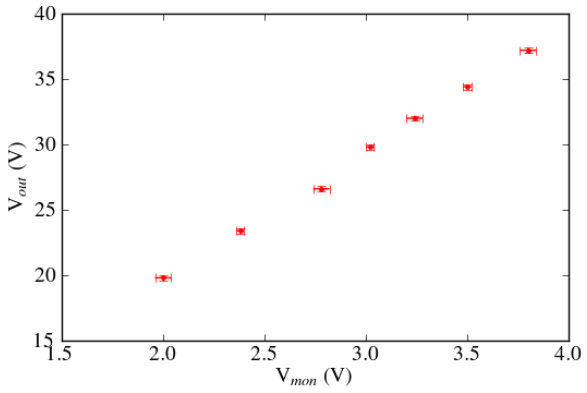

FIG. 7: Calibration of the PZT driver, showing the output voltage versus the monitor voltage.

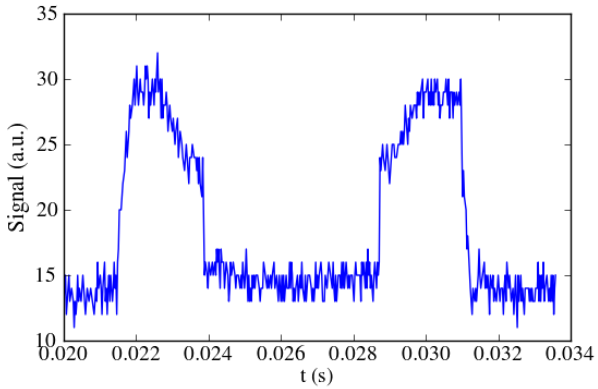

FIG. 8: Merlot-like features arising in the DPD signal when one of the arms is blocked.

fiber connected to the source stage, having an approximate waist of 1.08 mm and a power of 2.4 mW. This setup has the advantage of having a very good visibility, as the power in each of the arms should be the same (assuming perfect 50:50 beamsplitters). Small deviations can occur, in principle, if the beamsplitters are not perfect and if the reflectivity of the mirrors in each of the arms are different. We would also expect a slight dependence on polarization (a few percent) even if we are not dealing with polarizing beamsplitters, due to the imperfect nature of the coating.

Given that we are trying to measure phase changes on one of the arms that might be very small, we need to stabilize the MZI. There are several ways towards doing this, and many involve isolating each of the optical elements both thermally, acoustically and mechanically. However, we can use active feedback to achieve greater stability: if we have two beams passing through our interferometer, the probe beam and the reference beam, we can use feedback from from the reference signal (which, in principle, does not interact with our system) to drive the PZT and make sure that the path difference between both arms is constant. Using dichroic mirrors we would then be able to measure the phase shift undergone by the probe beam with a different set of photodetectors.

In our case, the mirror attached to the PZT is only 1/2-inch in diameter compared to the 1-inch in the other arm, thus we expect a small decrease in the amount of light reflected from that mirror. The choice of a 1/2 inch mirror is motivated by the need of reducing deformations in the mirror when it is being driven and the requirement of fast response of the PZT-mirror system, as a bigger mirror will have a greater inertia.

Introducing a thick glass plate in one of the arms and rotating it allows us to see fringes in the signal from the photodetector. As we move away from the position of zero optical path difference the visibility of the fringes is reduced as we are shifting the beam away from perfect overlap.

Apart from testing the stability of the MZI, we would like to know what is the shift in phase when we scan the frequency of the source.

Preliminary results show that the effect of scanning the frequency, using the PZT driving the grating on the source, is very small compared to the mechanical noise introduced, for example, when one enters the room.

We have also had the opportunity so see strange features when changing the input current of the laser: if we block one of the arms of the interferometer, we would expect to see a constant signal in the DPD when changing the current feeding the laser and sweeping across the spectrum, no matter what the intensity of the laser is, given a perfect 50-50 BS and no polarization dependence; however, we see merlon-like features arising where the mode-hops are found (see Figure 8).

When both paths are unblocked the signal increases, and the dynamics of the features as seen in the oscilloscope showed the plateaus arising in the mode hops were more stable in intensity than the surroundings when they were subject to mechanical or thermal noise. Misalignment was ruled out as the source of the features because these would be seen at every sweep in the piezo driving the grating, and not in particular values of the current drive. Introducing a quarter wave-plate before the last BS produced the results shown in Figure 9

Therefore, in order to avoid these discontinuities, we will work (as we were before) in regions where these features do not arise.

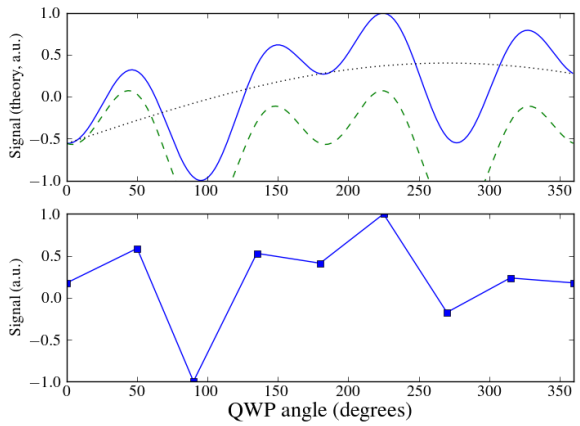

FIG. 9: Data points show the local minima and maxima of the features when scanning the angle of the QWP. The theoretical line (continuous) is the product $\sin(t)\sin(3t-0.5)$ plus a drift term, $\sin(t/3)$, shown in dashed and dotted lines, respectively. The drift term arises because of the delay in taking the data points; when taking it continuously, the drift term does not appear and the feature is 2π periodic.

D. Hybrid fiber-air

More flexibility in the MZI can be achieved if we could replace one of the arms of the interferometer with a fiber as can be seen in Figure 10. Our setup uses model PMJ-3AF3AF-780-5/125-3-6-1.

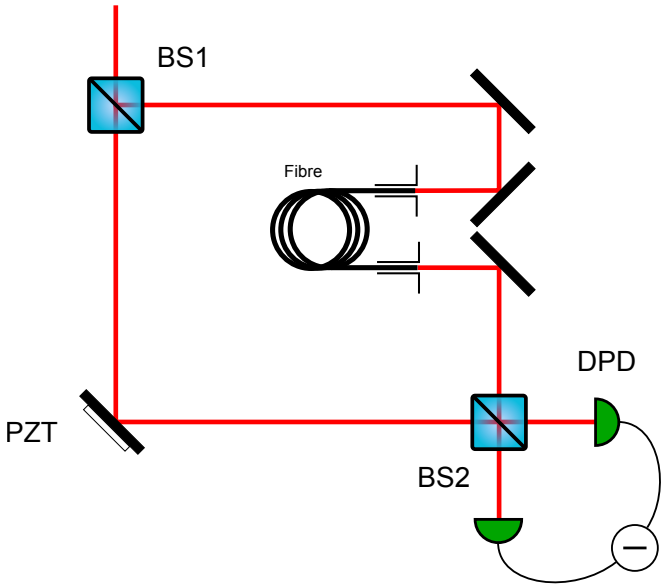

FIG. 10: Hybrid air-fiber MZI layout.

We expect to be able to stabilize the interferometer as in [6, 7]. However, the effects on the phase of thermal fluctuations and mechanical vibrations in the fiber have not yet been quantified in our experiment.

[1] B. L. Schumaker, Optics Letters **9** (May 1984).
[2] H. P. Yuen and V. W. S. Chan, Optics Letters **8** (March 1983).
[3] H. Pu, "Beam splitter and homodyne detection," `http://www.owlnet.rice.edu/~hpu/courses/Phys572_source/BSandHomodyne.pdf`.
[4] M. G. A. Paris, International Journal of Modern Physics B **11**, 1913 (1997).
[5] L. H. Tanner, Aeronautical Research Council (Reports and Memoranda **18733**, FM2463 (1956).
[6] D. C. Tardy, Rev. Sci. Instrum **64**, 623 (March 1993).
[7] S. A. Aljunid, M. K. Tey, B. Chng, T. Liew, G. Maslennikov, V. Scarani, and C. Kurtsiefer, Phys. Rev. Lett **103**, 153601 (2009).